3D-printed acoustic holograms to generate thermal holographic patterns

Diana Andrés, Jonathan Vappou, Noé Jiménez, et al.

Citation: Proc. Mtgs. Acoust. **48**, 020001 (2022); doi: 10.1121/2.0001635
View online: https://doi.org/10.1121/2.0001635
View Table of Contents: https://asa.scitation.org/toc/pma/48/1
Published by the Acoustical Society of America

ARTICLES YOU MAY BE INTERESTED IN

Use of simplified bowed string model in physics education: A laboratory experiment
Proceedings of Meetings on Acoustics **48**, 025001 (2022); https://doi.org/10.1121/2.0001628

A helicoidal parametric antenna for subwavelength vortex generation
Proceedings of Meetings on Acoustics **48**, 045001 (2022); https://doi.org/10.1121/2.0001629

Directional processing in assessment of wind turbine noise
Proceedings of Meetings on Acoustics **46**, 040002 (2022); https://doi.org/10.1121/2.0001637

Time-domain simulation of acoustic scattering and internal propagation from two gas bubbles
Proceedings of Meetings on Acoustics **46**, 022003 (2022); https://doi.org/10.1121/2.0001587

Simulation of near-ground signals from a flying source on UAV over a building structure
Proceedings of Meetings on Acoustics **46**, 045004 (2022); https://doi.org/10.1121/2.0001604



Advance your science and career
as a member of the
ACOUSTICAL SOCIETY OF AMERICA

LEARN MORE

Volume 48 http://acousticalsociety.org/

22nd International Symposium on Nonlinear Acoustics
Oxford, UK
4-8 July 2022

Biomedical Acoustics:
Session 8: General

3D-printed acoustic holograms to generate thermal holographic patterns

Diana Andrés
Instituto de Instrumentación para Imagen Molecular, Consejo Superior de Investigaciones Cientificas, Valencia, Valencia, 46022, SPAIN; diaanbau@upv.es

Jonathan Vappou
Université de Strasbourg, ICube, CNRS: Centre National de la Recherche Scientifique, Strasbourg, Grand Est, UMR7357, FRANCE; jvappou@unistra.fr

Noé Jiménez and Francisco Camarena
Instituto de Instrumentación para Imagen Molecular (i3M), Universitat Politècnica de València: Universitat Politecnica de Valencia, Valencia, 46022, SPAIN; nojigon@i3m.upv.es; fracafe@fis.upv.es

3D-printed holographic lenses coupled to an ultrasound transducer shape the acoustic field into arbitrary images. Predefined thermal patterns can be created with this technology in absorbing media, which can be used to generate localized and specific hyperthermia treatments. In this work we study how non-linearities in the acoustic field can affect the produced thermal pattern at hyperthermia intensity powers. A '2'-shaped acoustic hologram was designed with time-reversal methods and both acoustic and thermal numerical simulations were performed considering linear and non-linear propagation of the resulting acoustic field in liver-like medium. Experimental validation of the acoustic hologram was performed in degassed water, while the corresponding thermal pattern was evaluated using magnetic resonance thermometry and infra-red imaging in ex-vivo cow liver tissue and tissue-mimicking phantom. Simulations and experiments were in complete agreement, demonstrating that at hyperthermia intensities most of the energy is carried by the fundamental frequency and thus nonlinear propagation have little impact on resulting thermal pattern.

Published by the Acoustical Society of America

© 2022 Acoustical Society of America. https://doi.org/10.1121/2.0001635

1. INTRODUCTION

One of the most promising applications of biomedical ultrasound is the generation of mild and local hyperthermia. This emerging therapeutic procedure induces an increase in tissue temperature[1] from 40° C to 45° C, that has shown to have a great potential as radiosensitizer and enhancer for drug delivery.[2] In clinics, ultrasound hyperthermia is generated with phased arrays, which are high-cost and complex systems.[3]

While acoustic lenses have been used for decades in ultrasound transducers,[4] the recent advances in 3D printing technologies and rapid prototyping have triggered the interest in more accurate beam shaping strategies using passive structures, such as acoustic holograms.[5] Holograms have been applied for transcranial therapy to compensate skull aberrations and, simultaneously, generate complex focusing patterns[6,7] or single focal spots,[8] and recently were tested in-vivo for blood-brain barrier opening in mice,[9,10] used to create controlled cavitation patterns in homogeneous soft-tissue,[11] generated multiple patterns in homogeneous media,[12] multilayer holograms for phase and amplitude control,[13] optimized holograms,[14] or to conform vortex beams in homogeneous media[15] and in the brain.[16] Recently, it was presented how thermal patterns can be controlled using holograms in soft tissues to generate large-volume hyperthermia.[17]

In this work we study how nonlinearities in the acoustic field can affect the produced thermal pattern at hyperthermia intensity powers. As higher harmonics present a smaller wavelength, the nonlinear acoustic holograms should generate sharper images. However, the impact of these high-frequency components for the final thermal distribution remains unexplored. Thermal and acoustic numerical simulations were performed considering both linear and nonlinear propagation of the acoustic field in liver-like medium. Experimental acoustic and thermal measurements were done to validate these results using the designed 3D printed holographic lens. Acoustic measurements were done in degassed water with a needle hydrophone and thermal characterization was done in cow liver tissue and in gelatin-milk tissue mimicking phantom using an infrared (IR) camera and also with Magnetic Resonance (MR)-thermometry.

2. MATERIALS AND METHODS

With the purpose of designing thermal holographic patterns generated by ultrasound fields and evaluate their performance, we created an acoustic hologram with the shape of a number '2', located at 2 cm from a flat transducer surface. Hologram calculation was performed using a linear time-reversal method by setting virtual sources following the shape of the target image. The phase-conjugated information of the acoustic field produced by these sources was then captured at a surface parallel to the transducer, known as the holographic surface. This field was used to generate the target lens, as described by Jiménez-Gambín et al.[6] The holographic surface was divided into pixels of the same width and different height dependent on the recorded conjugated phase, assuming that each pixel vibrates presenting a longitudinal resonance mode.

Once the geometry of the lens is known, we calculated the resulting acoustic field using a pseudospectral time-domain simulation method,[18] considering both, linear and nonlinear propagation in the medium. Lens material properties were set to those corresponding to the Formlabs Clear resin, with density $\rho_L = 1171$ kg/m^3 and sound speed $c_L = 2580$ m/s. Attenuation was set to $\alpha_L = 2.72$ dB/(cm·MHz$^\gamma$), with $\gamma = 1.1$, as reported values for similar photopolymers.[5] A flat transducer of $2a = 50$ mm aperture and $f_0 = 1.1$ MHz central frequency was considered for the two-shaped hologram. All the medium in front of the transducer was set to liver tissue, with its acoustic properties (density $\rho_t = 1079$ kg/m^3,[19] sound speed $c_t = 1586$ m/s[20]). Acoustic attenuation in soft-tissue media was considered to follow a power-law frequency dependence as $\alpha_t = \alpha_0 \cdot f^\gamma$ where f is the ultrasound frequency, α_0 is the attenuation constant and $\gamma = 1.1$ is the power law exponent. As α_0 is frequency dependent, its value was 0.59 dB/(cm·MHz$^\gamma$), 1.32 dB/(cm·MHz$^\gamma$) and 1.98 dB/(cm·MHz$^\gamma$), for the first, second and third harmonic, respectively.[20] The parameter of nonlinearity in the medium was set to $B/A = 7.7$, according to existing literature.[21] Regarding the simulated domain size, the propagation path length was set to 50 mm (37 wavelengths at the central

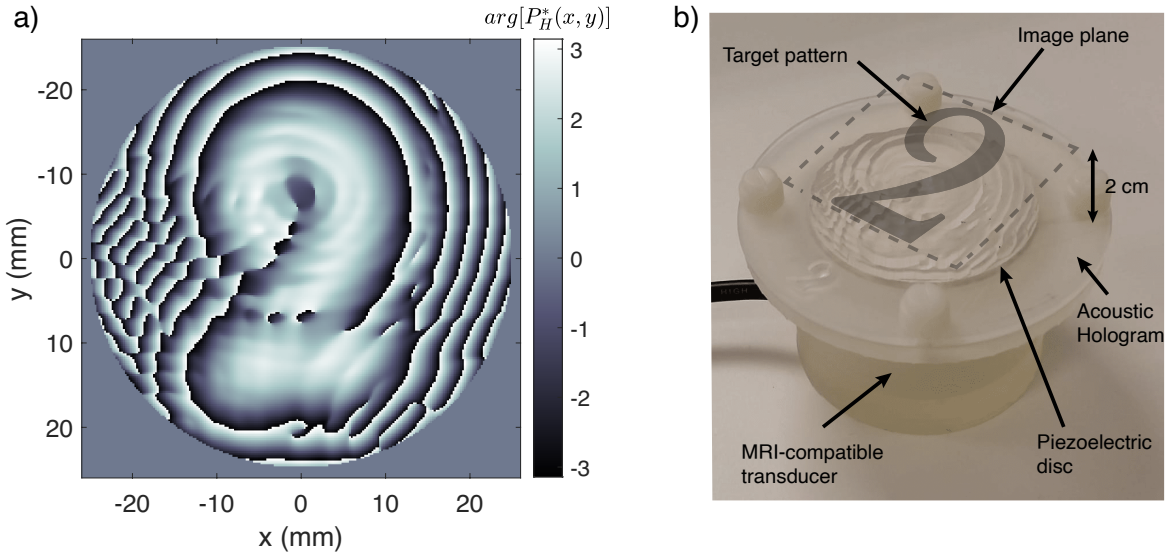


Figure 1: (a) Phase-conjugated field at the holographic surface (b) 3D-printed lens mounted in the custom-made MRI-compatible flat transducer.

frequency) and the domain width to 110 mm (82 wavelengths). A discretization of 6 points per wavelength for the third harmonic (f = 3.3 MHz) was used, and the Courant–Friedrichs–Lewy number was set to 0.2. Different acoustic pressures p_0 (0.35 MPa, 1.55 MPa and 4.5 MPa) at the transducer surface were modelled to study the power-dependence of the harmonic generation. Gol'dberg number was obtained to determine the propagation regime in each case, calculated as follows:[22]

$$\Gamma = \frac{\beta \omega p_0}{\alpha_t \rho_t c_t^3}, \tag{1}$$

Where β is the coefficient of nonlinearity ($\beta = 1 + B/2A$) and $\omega = 2\pi f_0$ is the angular frequency. Once the acoustic field is calculated, for both linear and nonlinear propagation, we obtained the resulting thermal pattern in liver tissue. Heat distribution was calculated with the Penne's bio-heat equation,[23] given by

$$\rho_t C_t \frac{\partial T}{\partial t} = \nabla(\kappa \nabla T) - W_b C_b (T - T_b) + Q, \tag{2}$$

where ρ_t, T, κ and C_t are the tissue density, temperature, thermal conductivity and specific heat capacity, W_b, T_b and C_b the blood perfusion rate, temperature and specific heat capacity, and Q the volume rate of heat deposition, defined as

$$Q = \sum_i 2\alpha_i I_i, \tag{3}$$

where the subindex $i = 1, 2, 3$ represents the harmonic number, α_i is the medium absorption coefficient at each harmonic and the intensity I_i is given by

$$I_i = \frac{p_i^2}{2\rho_t c_t}, \tag{4}$$

where p_i is the peak acoustic pressure at stationary state for each harmonic. In the case of linear propagation, peak pressure is calculated as the maximum pressure in steady state so no harmonic contributions appear. Blood perfusion was set to zero as experiments were done with ex-vivo tissues. Specific heat capacity and thermal conductivity were set to $C_t = 3540$ J/(kg·K) and $k = 0.52$ W/(m·K), according to values in the literature.[19]

A. EXPERIMENTAL SETUP

To validate numerical results for both acoustic field and thermal pattern, first the holographic lens was 3D printed with the desired material (Clear resin, Formlabs, USA). The lens designed to generate a two-shaped field was coupled to a custom-made MRI-compatible flat transducer of 50 mm apperture and 1.1 MHz central frequency with high temperature coupling gel (Sonotech Sono 600). Acoustic measurements were done in a degassed water tank at 23 °C. The system was driven by a 5-cycles sinusoidal pulse burst at the central frequency of the transducer with a signal generator (14 bits, 100 MS/s, model PXI5412, National Instruments, USA) and a linear RF amplifier (ENI 1040L, 400 W, 55 dB, ENI, Rochester, NY, USA). Pressure signals were measured with a piezoelectric hydrophone (-225.5 dB re 1 V/μPa at 1 MHz, Model Y-104, Sonic Concepts, USA), mounted in a 3D positioning system (10 μm precision, OWIS GmbH, Germany), in a region of 44 mm wide in both x and y dimensions, at $z = 20$ mm (at the holographic image location). Step size was set to 1 mm and each signal was averaged 20 times.

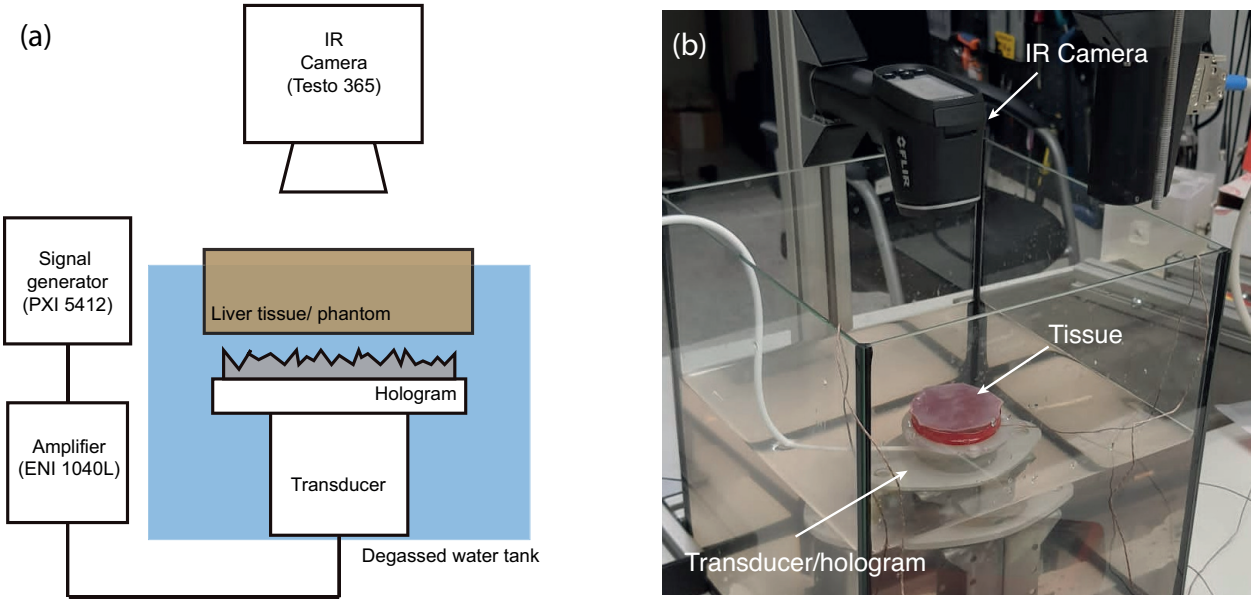


Figure 2: (a) Schematic diagram and (b) experimental setup for thermal measurements with infrared camera.

To study thermal holographic patterns generated by the lens in soft tissue medium two measurement systems were considered: IR camera and MR-thermometry. On the one hand, thermal hologram generated in the surface of a 20-mm slice of degassed ex-vivo cow liver tissue was obtained in time with the IR camera (FLIR TG165, Teledyne FLIR, USA). Images were obtained every 10 seconds while the transducer was driven with a continuous sinusoidal signal (duty cycle = 100%) at 1.1 MHz frequency and 25 W electrical power. It should be noted that there was no water between the camera and the flat surface of the liver tissue to prevent the infrared radiation to be absorbed, so a great impedance mismatch is found by the acoustic waves and all the energy will be reflected at the boundary. A picture of the experimental system is presented in Fig 2.

On the other hand, the same thermal pattern was monitored with Proton Resonance Frequency Shift MR-thermometry in a 1.5 T Aera MRI (Siemens, Erlangen, Germany) inside a piece of tissue mimicking phantom made of 4% gelatin and 30% concentrated milk, to prevent this liver-air boundary. Thermal images were obtained inside the phantom every 1.2 seconds, with a lateral resolution of 2 mm.

3. RESULTS

A. ACOUSTIC HOLOGRAM

The acoustic hologram was first simulated in linear and nonlinear regime to study the possible nonlinear effects at high pressure amplitudes needed for ultrasound hyperthermia. Three different pressure amplitudes at the surface transducer were considered: 0.3, 1.5 and 4.5 MPa, resulting in peak pressures of 1.2, 7.1 and 29 MPa at the acoustic holographic image plane, which corresponds to mechanical indexes of 1.1, 4.9 and 12.6, respectively. Gol'dberg number of these three different regimes was 3.6, 17.9 and 53.7, respectively. As expected, contribution of harmonics to the acoustic field was significant at higher pressures: for 0.3 MPa source amplitude, only 4% of the total energy is carried by the second harmonic and 0.25% by the third harmonic, while for the 1.5 MPa case percentages of the total energy carried by the second and third harmonic were 15.5% and 3%, or for the 4.5 MPa case these same proportions were of 27% and 18%. Also, higher harmonics contribute to generate a sharper image, with more resolution (see Fig. 3).

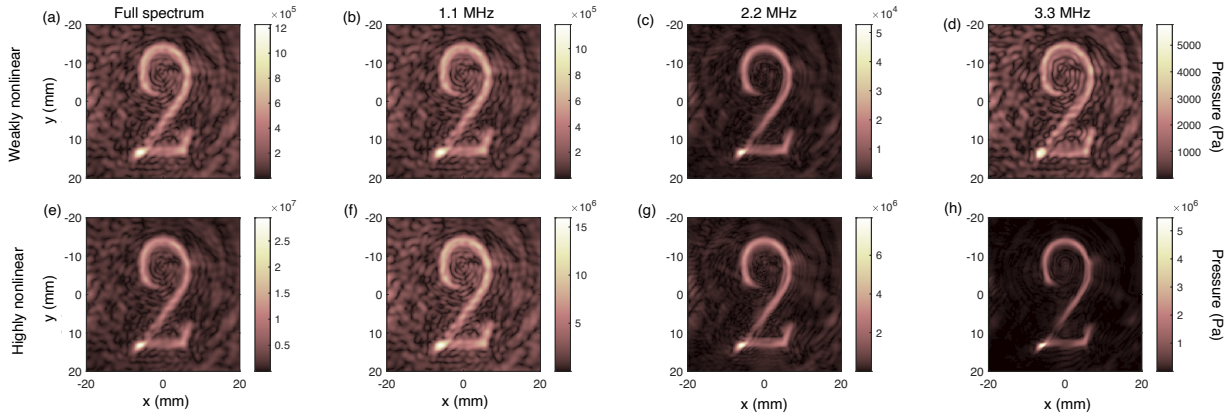


Figure 3: (a-d) Peak pressure considering the full spectrum and spectral decomposition for 0.3 MPa at the transducer surface. (e-h) Full spectrum and spectral decomposition for 4.5 MPa at the transducer surface. Note each figure has its own colour scale.

Experimental evaluation of the acoustic field was done with the system described in the *Materials and Methods* section. Peak pressure values in steady state at the image plane measured by the needle hydrophone are represented in Fig. 5 (a). Both experimental and acoustic field corresponding to the full-spectrum weakly nonlinear regime (Fig. 3 (a)) were compared. In the region of the target image, relative error between both experimental and simulated fields is much lower than in the outer region, where random noise increases the error. Relative error was calculated as

$$\epsilon(\%) = \frac{p_{\text{exp}}/\max(p_{\text{exp}}) - p_{\text{sim}}/\max(p_{\text{sim}})}{p_{\text{sim}}/\max(p_{\text{sim}})} \times 100, \tag{5}$$

where p_{exp} and p_{sim} are the measured and simulated pressure fields respectively. Average relative error in the region of interest (without considering random noise) is 31%.

B. THERMAL HOLOGRAPHIC PATTERN IN THE WEAKLY-NONLINEAR REGIME

Thermal holographic pattern generated by the acoustic hologram would also depend on the contribution of each harmonic with its peak pressure, as the heating source term depends on the quadratic pressure of each harmonic and also on the attenuation, which increases with the harmonic order. Calculations show that for the higher pressure studied, nonlinear effects makes a slight difference with the linear pattern,

which becomes more important in the regions of high pressure. The highest difference between linear and nonlinear thermal pattern is of 18% (relative to the nonlinear field) while average difference at the region of interest is 8.2%. Nevertheless, for hyperthermia applications, where maximum desired temperatures are of 45° C, pressure fields are in the weakly nonlinear regime, where no difference in the thermal pattern is found between linear and nonlinear propagation (Fig. 4 (b)). Also, thermal patterns are dominated by heating diffusion, so the image blurs with time and is not as sharp and stable as the acoustic hologram.

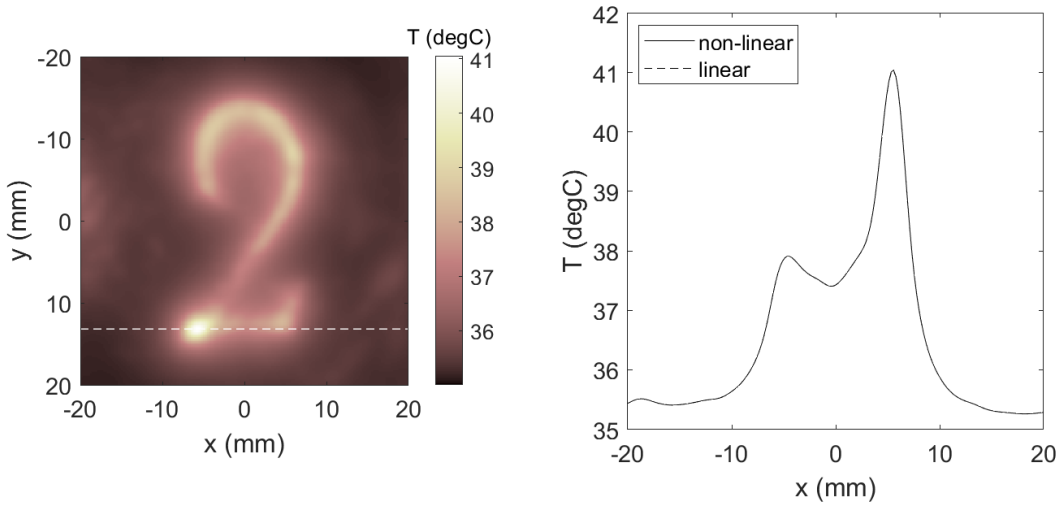


Figure 4: (a) Simulated thermal pattern for 0.3 MPa at the transducer surface (white dashed line represents location of lineal cuts). (b) Lineal cut for linear (dashed line) and nonlinear (solid line) propagation at 0.3 MPa.

Thermal measurement done with the IR-camera in the surface of a piece of ex-vivo cow liver tissue is shown in Fig. 5 (b). Thermal image matches the simulated one in weakly nonlinear regime (Fig. 4 (a)), showing a temperature rise of $\Delta T = 4.5°$ C after 12 seconds heating with continuous signal at 20 W. After one minute heating, thermal image becomes blurred and heat is transported towards the edges of the ex-vivo tissue. To evaluate thermal pattern without the high impedance mismatch condition at the image plane, same measurements were also done using MRI-thermometry inside liver-mimicking phantom. Ultrasound heating was performed with the transducer driven with continuous signal at 40 W acoustic power, leading to a temperature rise of $\Delta T = 15°$ C after 40 seconds of heating (Fig. 4 (c)). Temperature differences between both experiments depend mainly on the electrical power input but also on the tissue properties and boundary conditions: MRI measurements were made in the bulk of a piece of gelatin-milk phantom while infrared measurements were made at the surface of a piece of cow liver tissue, at the interface between water and air. Nevertheless, both thermal experimental measurements demonstrate that a predefined thermal holographic pattern can be generated using ultrasound holograms, showing its robustness to generate thermal patterns inside absorbing media as soft tissue.

4. CONCLUSION

In this work we have proven that in the nonlinear regime higher harmonics can enhance the spatial resolution of acoustic holograms, creating sharper acoustic images as driving power increases. Nevertheless, for mild hyperthermia applications, nonlinear propagation is weak and have little impact on resulting thermal patterns because most of the energy is carried by the fundamental frequency. Even considering that the

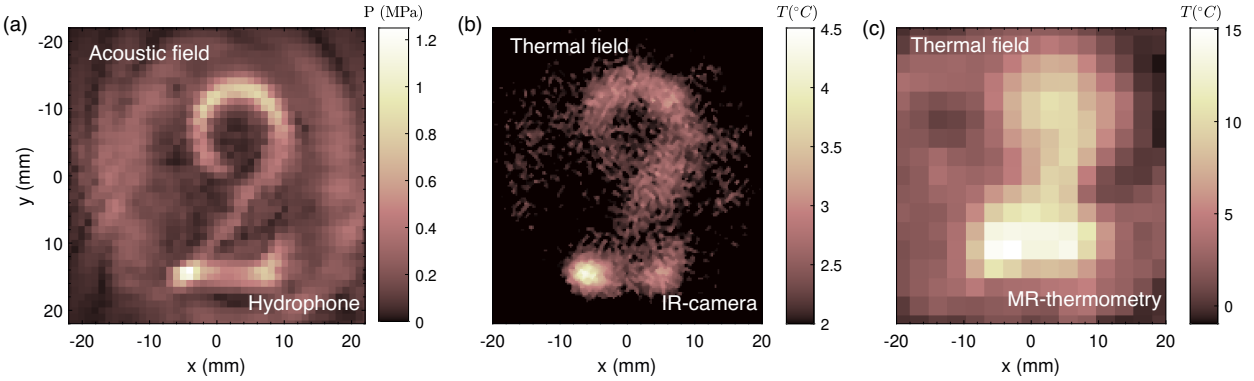


Figure 5: (a) Experimental acoustic field. (b) Experimental thermal field measured with infrared camera. (c) Experimental thermal field measured with MR-thermometry.

absorption is higher for higher harmonics, the heating source is dominated by the fundamental component, and we do not observe any improvement in the resolution of the thermal pattern. Experimental validation was performed using an ex-vivo tissue and tissue mimicking gelatin-milk phantom with infrared imaging and MR-thermometry, showing great agreement with simulations. These results demonstrate the ability of holographic lenses coupled to flat ultrasound transducers to create arbitrary-shaped thermal patterns in absorbing media. It remains unexplored how blood perfusion affects thermal holographic patterns for in-vivo applications, or how lens heating affects polymer stability during continuous driving for hyperthermia treatments. However, we have demonstrated a proof of concept that this technology can be used to shape the acoustic field of existing devices, or to match the shape of the thermal hologram to complex target regions for hyperthermia applications.

ACKNOWLEDGMENTS

This research has been supported by the Spanish Ministry of Science, Innovation and Universities (MICINN) through grants IJC2018-037897-I, FPU19/00601 and PID2019-111436RB-C22, by the Agència Valenciana de la Innovació through grants INNCON/2021/8 and INNVA1/2020/92, by Generalitat Valenciana through grant AICO/2020/268. Action co-financed by the European Union through the Programa Operativo del Fondo Europeo de Desarrollo Regional (FEDER) of the Comunitat Valenciana 2014-2020 (IDIFEDER/2018/022) and (IDIFEDER/2021/004). Action co-financed by BPI France, Région Grand Est and FEDER (UFOGUIDE project).

REFERENCES

[1] L. Zhu, M. B. Altman, A. Laszlo, W. Straube, I. Zoberi, D. E. Hallahan, and H. Chen, "Ultrasound hyperthermia technology for radiosensitization," *Ultrasound in medicine & biology*, vol. 45, no. 5, pp. 1025–1043, 2019.

[2] J. P. May and S.-D. Li, "Hyperthermia-induced drug targeting," *Expert opinion on drug delivery*, vol. 10, no. 4, pp. 511–527, 2013.

[3] M. Thanou and W. Gedroyc, "Mri-guided focused ultrasound as a new method of drug delivery," *Journal of drug delivery*, vol. 2013, 2013.

[4] R. J. Lalonde, A. Worthington, and J. W. Hunt, "Field conjugate acoustic lenses for ultrasound hyperthermia," *IEEE transactions on ultrasonics, ferroelectrics, and frequency control*, vol. 40, no. 5, pp. 592–602, 1993.

[5] K. Melde, A. G. Mark, T. Qiu, and P. Fischer, "Holograms for acoustics," *Nature*, vol. 537, no. 7621, pp. 518–522, 2016.

[6] S. Jiménez-Gambín, N. Jiménez, J. M. Benlloch, and F. Camarena, "Holograms to focus arbitrary ultrasonic fields through the skull," *Physical Review Applied*, vol. 12, no. 1, p. 014016, 2019.

[7] D. Andrés, N. Jiménez, J. M. Benlloch, and F. Camarena, "Numerical study of acoustic holograms for deep-brain targeting through the temporal bone window," *Ultrasound in Medicine & Biology*, vol. 48, no. 5, pp. 872–886, 2022.

[8] G. Maimbourg, A. Houdouin, T. Deffieux, M. Tanter, and J.-F. Aubry, "3d-printed adaptive acoustic lens as a disruptive technology for transcranial ultrasound therapy using single-element transducers," *Physics in Medicine & Biology*, vol. 63, no. 2, p. 025026, 2018.

[9] S. Jiménez-Gambín, N. Jiménez, A. N. Pouliopoulos, J. M. Benlloch, E. E. Konofagou, and F. Camarena, "Acoustic holograms for bilateral blood-brain barrier opening in a mouse model," *IEEE Transactions on Biomedical Engineering*, vol. 69, no. 4, pp. 1359–1368, 2021.

[10] J. He, J. Wu, Y. Zhu, Y. Chen, M. Yuan, L. Zeng, and X. Ji, "Multitarget transcranial ultrasound therapy in small animals based on phase-only acoustic holographic lens," *IEEE Transactions on Ultrasonics, Ferroelectrics, and Frequency Control*, vol. 69, no. 2, pp. 662–671, 2021.

[11] J. Kim, S. Kasoji, P. G. Durham, and P. A. Dayton, "Acoustic holograms for directing arbitrary cavitation patterns," *Applied Physics Letters*, vol. 118, no. 5, p. 051902, 2021.

[12] M. D. Brown, B. T. Cox, and B. E. Treeby, "Stackable acoustic holograms," *Applied Physics Letters*, vol. 116, no. 26, p. 261901, 2020.

[13] M. D. Brown, "Phase and amplitude modulation with acoustic holograms," *Applied Physics Letters*, vol. 115, no. 5, p. 053701, 2019.

[14] T. Fushimi, K. Yamamoto, and Y. Ochiai, "Acoustic hologram optimisation using automatic differentiation," *Scientific reports*, vol. 11, no. 1, pp. 1–10, 2021.

[15] S. Jiménez-Gambín, N. Jiménez, J. M. Benlloch, and F. Camarena, "Generating bessel beams with broad depth-of-field by using phase-only acoustic holograms," *Scientific reports*, vol. 9, no. 1, pp. 1–13, 2019.

[16] S. Jiménez-Gambín, N. Jiménez, and F. Camarena, "Transcranial focusing of ultrasonic vortices by acoustic holograms," *Physical Review Applied*, vol. 14, no. 5, p. 054070, 2020.

[17] D. Andrés, J. Vappou, N. Jiménez, and F. Camarena, "Thermal holographic patterns for ultrasound hyperthermia," *Applied Physics Letters*, vol. 120, no. 8, p. 084102, 2022.

[18] B. E. Treeby, J. Jaros, A. P. Rendell, and B. Cox, "Modeling nonlinear ultrasound propagation in heterogeneous media with power law absorption using ak-space pseudospectral method," *The Journal of the Acoustical Society of America*, vol. 131, no. 6, pp. 4324–4336, 2012.

[19] R. L. Mcintosh and V. Anderson, "A comprehensive tissue properties database provided for the thermal assessment of a human at rest," *Biophysical Reviews and Letters*, vol. 5, no. 03, pp. 129–151, 2010.

[20] B. E. Hammer, "Physical properties of tissues," *Radiology*, vol. 181, no. 1, pp. 128–128, 1991.

[21] E. Jackson, C. Coussios, and R. Cleveland, "Nonlinear acoustic properties of ex vivo bovine liver and the effects of temperature and denaturation," *Physics in Medicine & Biology*, vol. 59, no. 12, p. 3223, 2014.

[22] M. F. Hamilton, "Effective gol'dberg number for diverging waves," *The Journal of the Acoustical Society of America*, vol. 140, no. 6, pp. 4419–4427, 2016.

[23] H. H. Pennes, "Analysis of tissue and arterial blood temperatures in the resting human forearm," *Journal of applied physiology*, vol. 1, no. 2, pp. 93–122, 1948.